Catalysis Today 169 (2011) 242–248

Contents lists available at ScienceDirect

Catalysis Today

journal homepage: www.elsevier.com/locate/cattod

Vanadium and antimony supported $NbSiO_x$—Characterisation and catalytic properties in methanol oxidation☆

Hanna Golinska, Piotr Decyk, Maria Ziolek*

Adam Mickiewicz University, Faculty of Chemistry, Grunwaldzka 6, 60-780 Poznań, Poland

ARTICLE INFO

Article history:
Available online 1 September 2010

Keywords:
$VSb/NbSiO_x$
Acid–base properties
Selective oxidation
Methanol

ABSTRACT

Niobosilica material ($NbSiO_x$) prepared by a simple method without the use of organic template was applied as a support for $SbVO_x$ phases with high Sb and V contents. In this paper we describe the preparation of $VSb/NbSiO_x$ catalysts, their structural/textural characterisation (studied by XRD, N_2 adsorption, UV–vis, ESR) and surface catalytic properties (estimated from pyridine adsorption, test reactions: acetonylacetone cyclisation and methanol oxidation). It was found that vanadium–antimony binary oxide phase interacts with acidic hydroxyls on $NbSiO_x$ surface. Such interaction leads to the formation of $Sb_{0.95}V_{0.95}O_4$ rutile phase and new OH groups exhibiting basic properties. As the strength of interaction of $Sb_{0.95}V_{0.95}O_4$ phase with niobium species in $NbSiO_x$ support increases with increasing calcination temperature, the particle sizes of rutile phase are smaller for higher calcination temperatures. High calcination temperatures cause that more vanadium species are present at the +4 oxidation state, whereas after low-calcination temperatures and at high vanadium content V=O species are formed and they are well visible in UV–vis spectra of the catalysts. The presence and role of different active centres on $VSb/NbSiO_x$ catalysts are discussed on the basis of results obtained in the oxidation of methanol.

1. Introduction

Methanol is one of the most important chemical intermediates used in industrial chemistry. It is the starting reactant for synthesis of various products, including hydrocarbons and mild oxidation products. Among the oxidation processes, formaldehyde production for the synthesis of phenolic resins [1] is largely predominant. The catalytic methanol oxidation at low temperature can be also applied as a good test reaction to characterise the surface properties of oxide catalysts [1–7]. The gas-phase partial oxidation of methanol is an important probe reaction, whose product selectivity depends on the concentration of redox, basic and acidic sites on the catalyst surface [1–3,6].

The mechanism of methanol oxidation can be considered on the basis of literature [e.g. [1–7]]. Catalytic oxidation of methanol requires the formation of chemisorbed methoxy groups, which are further transformed to formaldehyde species as a result of extraction of hydrogen from CH_3 by activated oxygen [3,4,7]. Acidic and basic sites are required in the formation of methoxy species, whereas the redox sites on the catalyst surface are involved in the transformation of methoxy groups towards formaldehyde [1,3,4]. If formaldehyde is chemisorbed on nucleophilic species strongly enough, it can interact with another methanol molecule and form methyl formate [1,3]. Methanol can be also chemisorbed on pairs of active centres giving rise to formate species, which further interact with methanol to methyl formate. Of course, the total oxidation of methanol to CO_2, which usually involves basic centres, is also possible [1]. The observed reaction products depend on the possibility of formation of the intermediates desired and the strength of their chemisorption. The type of intermediates is determined by the surface properties of the catalyst [2].

Various metal oxides and mixed metal oxides have been already used in methanol oxidation. The binary oxides in which vanadium species are expected to be active centres (vanadium(V) oxide with oxides of Sb, Co, Cr, Pb, Bi, Zn, Mg) belong to the catalysts widely studied in oxidative dehydrogenation of alkanes [8]. It has been frequently observed that the addition of the second oxide which is itself inactive or unselective for the oxidation reaction is able to improve the activity of the primary oxide substantially [7]. Such inactive oxide exhibiting donor properties is Sb_2O_4. Delmon et al. [9] described spillover of oxygen adsorbed dissociatively on Sb_2O_4 from which oxygen atoms diffuse to the primary oxide (in their work it was SnO_2). The same phenomenon can be expected

☆ The paper is dedicated to the memory of late Prof. Haber, a great scientist and authority on catalysis, kind teacher and friend to whom MZ is personally much indebted. We appreciate his passion, knowledge, and openness for discussion and resolving scientific problems. His work and personality will long be remembered.

* Corresponding author. Tel.: +48 61 8291243.
E-mail address: ziolek@amu.edu.pl (M. Ziolek).

0920-5861/$ – see front matter © 2010 Elsevier B.V. All rights reserved.
doi:10.1016/j.cattod.2010.07.025

if V_2O_5 is used as acceptor oxide. The binary metal oxides like $SbVO_x$ can be attractive for oxidative dehydrogenation of alcohols. At present vanadium–antimony catalysts are well known as promising for ammoxidation processes [e.g. [10–14]]. However, they were also used in selective oxidation of methanol to formaldehyde. Li and coworkers [15] used $VSbO_x/SiO_2$ for methanol oxidation to formaldehyde and found that Sb–V mixed oxides are more selective than vanadia supported on silica because the relative amount of monomeric VO_x species is higher in mixed oxides.

Recently, our interest has been focused on various hexagonally ordered mesoporous materials containing niobium applied in oxidation of methanol [2,16–18]. Niobium compounds exhibit special properties not shown by the compounds of neighbouring elements in the periodic table. Some of these properties, like strong metal support interaction (SMSI) or unique reversible interaction with several reagents, are very important for the design of catalysts. We have used NbMCM-41 materials as supports for vanadium and antimony mixed oxides [19] which appeared to be interesting catalysts in ammoxidation reactions [20]. When high loading of $SbVO_x$ was applied the hexagonal ordering of MCM-41 materials was destroyed. Therefore, the aim of this study was to use a non ordered niobosilica material prepared by a simple method without the use of organic template, according to [21], as a support for high loading of $SbVO_x$. In this paper we describe the preparation of such supported catalysts, their structural/textural characterisation and surface catalytic properties, mainly in the oxidation of methanol, which could allow further design of catalysts to be applied in oxidation and ammoxidation of alcohols and hydrocarbons.

2. Experimental

Niobiosilica $NbSiO_x$ was prepared in water by co-precipitation (*aqueous route* synthesis). Aqueous solution of $C_4H_4NNbO_9$ (Aldrich) was gently dropped into TEOS, previously hydrolyzed with hydrochloric acid (0.05 M) at room temperature for ca. 60 min. The HCl/TEOS molar ratio was kept constant to 4. The amounts of Nb and Si sources were calculated for Si/Nb ratio equal to 64. Then, ammonia aqua solution (28 mass%) was added dropwise to the obtained limpid solution, until complete precipitation. The solid was aged at room temperature for 24 h, dried under vacuum at 313 K for 2 h, and calcined at 823 K for 8 h.

Commercial silica, SiO_2 (Degussa AG D-60287) was used as a reference support for catalysts.

Both $NbSiO_x$ and SiO_2 samples were modified by the wetness impregnation with vanadium and antimony. Various V/Sb molar ratios were applied. The procedure of modification with Sb and V included the stepwise impregnation with antimony and vanadium precursors ($(CH_3COO)_3Sb$) and NH_4VO_3, respectively) using V/Sb atomic ratios of 1 or 0.5 and ~25 wt.% of Sb. NH_4VO_3 (BDH Chemicals Ltd.) was dissolved in H_2O and $(CH_3COO)_3Sb$ (Aldrich) was dissolved in tartaric acid (0.3 M). The amounts of both solutions accounted for 25 wt.% of Sb and 5 wt.% of V loading giving rise to V/Sb = 0.5 atomic ratio (the samples denoted $0.5VSb/NbSiO_x$ and $0.5VSb/SiO_2$) and 25 wt.% of Sb and 10 wt.% of V loading leading to V/Sb = 1 atomic ratio (the sample denoted $1VSb/NbSiO_x$). The outgased calcined mesoporous material (353 K, 1 h in evaporator) was filled in with the appropriate amount of an tartaric acid solution of Sb precursor and placed in an evaporator flask, where the catalyst was rotated and next heated in oven at 353 K for ca. 12 h. After such drying the following impregnation by the admission of aqueous solution of NH_4VO_3 was carried out. Finally the catalyst was dried at 353 K for 12 h and calcined in air at 923 K for 96 h or at 813 K for 6 h (the sample marked as $0.5VSb/NbSiO_x(813)$).

$Sb_{0.95}V_{0.95}O_4$ described in [10] was obtained by drying in a rotatory evaporator at 353 K an aqueous solution of NH_4VO_3 and $(CH_3COO)_3Sb$) in 0.3 M tartaric acid; the amounts of precursors for V and Sb were determined to have a nominal Sb/V atomic ratio of 1. The resulting solid was dried at 353 K for 24 h and then calcined at 813 K for 6 h.

To establish the Si/Nb or Si/V or Si/Sb ratio X-ray fluorescence (XRF) was applied using MiniPal – Philips apparatus. The measurements were done using calibration curves based on the XRF measurements for the prepared mixtures from silica (Degussa) and Nb_2O_5 (Alfa Aesar) or V_2O_5 (Aldrich) or Sb_2O_3 (Aldrich) (Si/V or Si/Sb from 1 to 300).

The prepared materials were characterized by XRD (D8 Advance, Bruker diffractometer) with the use of CuKα radiation ($\lambda = 0.154$ nm).

The surface area and pore volume of the catalysts were estimated by nitrogen adsorption at 77 K using the conventional technique on a Micromeritics 2010 apparatus. Prior to the adsorption measurements, the samples were degassed in vacuum at 573 K for 2 h.

UV–vis spectra were registered using a Varian-Cary 300 Scan UV–visible spectrophotometer. Catalyst powders were placed into the cell equipped with a quartz window. The Kubelka–Munk function (F(R)) was used to convert reflectance measurements into equivalent absorption spectra using the reflectance of SPECTRALON as a reference.

The electron spin resonance (ESR) study was performed at 77 K using RADIOPAN SE/X 2547 spectrometer. A cavity operating at a frequency of 8.9 GHz (X-band) with 100 kHz field modulation was used.

Surface properties of prepared materials were studied by in situ FT-IR spectroscopy of pyridine adsorbed. Self-supporting pellets of around 10 mg cm^{-2} were prepared and located in a classical glass cell connected to a vacuum-adsorption apparatus for in situ experiments. IR spectra were recorded at room temperature with a Bruker Vector 22 FT-IR spectrometer (resolution 4 cm^{-1}). All the samples were activated in situ at 673 K under vacuum before any characterisation. Pyridine was adsorbed at 373 K and evacuated at various temperatures (373–523 K) for 30 min at each temperature. The IR spectra of the activated samples were subtracted from those registered after the adsorption of pyridine. The reported spectra are the results of this subtraction.

The catalysts were tested in acetonylacetone (AcOAc) cyclisation as the probe reaction. A tubular, down-flow reactor was used in AcOAc cyclisation reaction that was carried out at atmospheric pressure, using nitrogen as the carrier gas. The catalyst bed (0.05 g) was first activated for 2 h at 673 K under nitrogen flow (40 cm^3 min^{-1}). Subsequently, a 0.5 cm^3 of acetonylacetone (Fluka, GC grade) was passed continuously into the catalyst at 623 K. The substrate was delivered with a pump system and vaporized before being passed through the catalyst with the flow of nitrogen carrier gas (40 cm^3 min^{-1}). The reaction products were collected for 30 min downstream of the reactor in the cold trap (liquid nitrogen + 2-propanol) and analysed by gas chromatography (CHROM-5, Silicone SE-30/Chromosorb column).

The methanol oxidation reaction was performed in a fixed-bed flow reactor. 0.03 g of the pure (not diluted) catalyst, with a size fraction of $0.5 < Ø < 1$ mm, was placed into the reactor. The samples were activated in helium flow (40 cm^3 min^{-1}) at 673 K for 2 h (the rate of heating was 15 K min^{-1}). Next the temperature decreased to the temperature of the reaction. A 40 cm^3 min^{-1} He/O_2/MeOH (88/8/4 mol%) flow was used as a reactant mixture. The reactor effluent was analysed using an on line gas chromatograph (GC 8000 Top equipped with a capillary column of DB-1 – FID detector and Porapak Q and 5A molecular sieves columns – TCD detector). Helium was applied as a carrier gas.

Table 1
Texture/structure parameters.

Catalyst	Surface area BET [m^2/g]	Pore volume BJH [cm^3/g]	$Sb_{0.95}V_{0.95}O_4$ size (XRD) [nm]		Nb/Si (XRF)	V/Si (XRF)	Sb/Si (XRF)
			2Θ = 27.4 (1 1 0)	2Θ = 53.4 (2 1 1)			
$NbSiO_x$	165	0.9	–	–	0.016	–	–
0.5VSb/$NbSiO_x$	92	0.3	40	28	0.016	0.025	0.149
0.5VSb/$NbSiO_x$(813)	74	0.3	44	36	0.016	0.023	0.179
1VSb/$NbSiO_x$	18	0.1	41	33	0.016	0.072	0.108
SiO_2	176	–	–	–	–	–	–
0.5VSb/SiO_2	67	0.4	32	23	–	0.023	0.166
$Sb_{0.95}V_{0.95}O_4$	13	0.4	34	31	–	–	–

3. Results and discussion

3.1. Textural/structural characterisation

Chemical composition and textural parameters of the samples studied (the supports and materials containing Sb and V) based on XRF measurements and nitrogen adsorption isotherms are shown in Table 1. For comparison the parameters of $Sb_{0.95}V_{0.95}O_4$ bulk phase are also given. Surface area and pore volume significantly decrease after impregnation with antimony and vanadium source.

The XRD patterns of niobia-silicate $NbSiO_x$ materials (Fig. 1A(g)) show very broad and low intensity peaks around $2\theta \sim 15^\circ$ to 25°, typical of the presence of unstructured silica. No other XRD reflexes are visible. It indicates that neither Nb_2O_5 nor any other niobium oxide phase is present on the support in the amount detectable by XRD. For 0.5VSb/$NbSiO_x$ (Fig. 1A(a)), well visible forms of Sb–V–O_x crystalline bimetallic oxides are detected and the observed XRD peaks could be assigned to rutile $Sb_{0.95}V_{0.95}O_4$ (JCPDS 16-0600) structure. However, the positions of XRD peaks are shifted relative to those from the catalogue (Fig. 1A(f)). The same phenomenon is noted for all antimony-vanadium species loaded on $NbSiO_x$ (Fig. 1A(a), (b), and (d)). This effect can be attributed to a distortion in the lattice of the Sb–V–O phase resulting from the interaction with the support as it was reported for the vanadium–antimony phase spread on alumina [10]. Interestingly, when $Sb_{0.95}V_{0.95}O_4$ phase is loaded on silica (Fig. 1A(c)) the positions of XRD peaks are exactly the same as those from the catalogue (Fig. 1A(f)). Similarly like in the case of alumina, niobiosilica material have much higher concentration of OH groups on the surface than SiO_2 which is demonstrated by the much higher intensity of IR band at 3746 cm^{-1} on $NbSiO_x$ than on SiO_2 (Fig. 1B). Niobium present in the support is responsible for the creation of OH groups and interaction with rutile phase and a distortion in the lattice of the Sb–V–O phase. Such interaction seems to influence the particle size of the rutile vanadium–antimony–oxide phase which is smaller when silica is used as the support (0.5VSb/SiO_2 – Table 1) than when $NbSiO_x$ plays the role of the support. Similar behaviour was found when vanadium–antimony phase was loaded on mesoporous materials containing niobium or without niobium [20]. Table 1 reveals two values of particle sizes calculated from two various XRD peaks. The slight differences between them indicate different distribution of crystal faces accessible for X-ray diffraction. However, the general tendency of changes in the crystallite sizes is the same for both faces analysed. Interestingly, the temperature and time of heating determine the particle size of rutile phase. The lower the temperature of calcination (813 K – the sample 0.5VSb/$NbSiO_x$(813)) the greater particles are formed. Most probably at the higher temperature the interaction between $Sb_{0.95}V_{0.95}O_4$ and niobium is greater and the stronger anchored $SbVO_x$ molecules prevent formation of agglomerations of rutile crystals, which means that the particle are smaller. XRD patterns of oxide structures such as Sb_2O_3, Sb_2O_4 or V_2O_5 were not detected.

The temperature and time of the catalyst calcination as well as vanadium content influence the coordination of vanadium in vanadium–antimony rutile phase as deduced from UV–vis study. According to literature [22–25] the UV–vis region examined is asso-

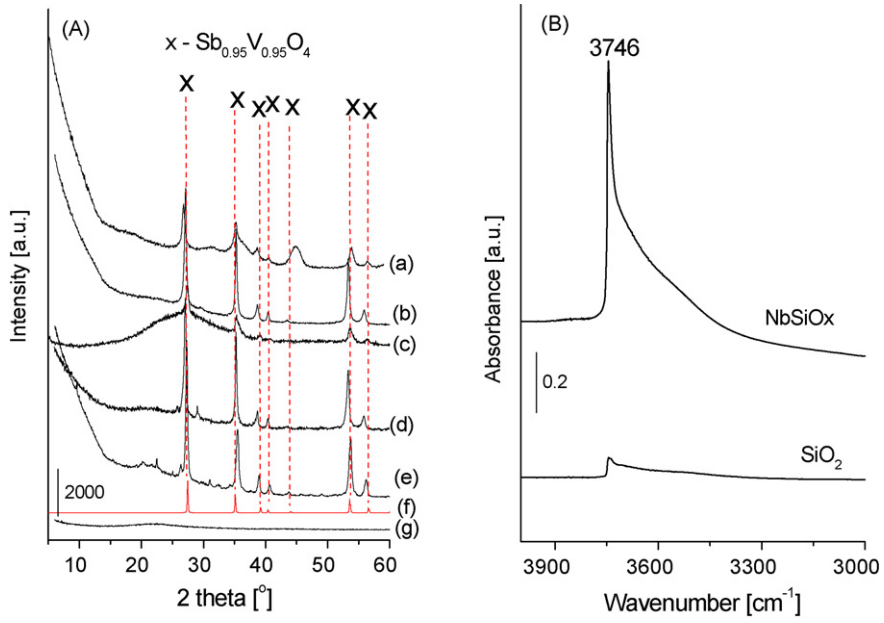

Fig. 1. (A) XRD patterns of: (a) 0.5VSb/$NbSiO_x$; (b) 1VSb/$NbSiO_x$; (c) 0.5VSb/SiO_2; (d) 0.5VSb/$NbSiO_x$ (813); (e) $Sb_{0.95}V_{0.95}O_4$; (f) $Sb_{0.95}V_{0.95}O_4$ (JCPDS 16-0600); (g) $NbSiO_x$ and (B) FT-IR spectra of supports after evacuation for 3 h at 673 K.

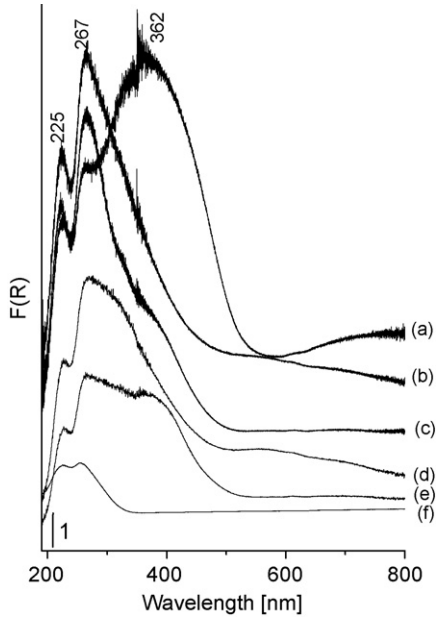

Fig. 2. UV–vis spectra of: (a) $Sb_{0.95}V_{0.95}O_4$; (b) 0.5VSb/SiO_2; (c) 0.5VSb/$NbSiO_x$ (813), (d) 0.5VSb/$NbSiO_x$; (e) 1VSb/$NbSiO_x$; (f) $NbSiO_x$.

ciated with the transfer of electron from oxygen to the transition metal. For niobium(V) tetrahedral species located in the silicate matrix the UV bands usually appear at ~225 and ~250 nm [16]. In fact, Fig. 2f shows UV bands at such positions for $NbSiO_x$ support. The same bands are observed after Sb–V–O_x loading with vanadium–antimony phase, but the band at 267 nm is much more pronounced after $NbSiO_x$ modification. The reason is that this band is overlapped with that assigned to the oxygen–tetrahedral V(V) charge transfer (CT) transitions, involving bridging (V–O–Si) oxygen. A shoulder at ca. 360 nm, especially well visible in the spectra of 0.5VSb/$NbSiO_x$(813) and 1VSb/$NbSiO_x$ (Fig. 2c and e), i.e. the samples calcined at lower temperature (813 K) and of higher content of vanadium, is assigned to the electron transfer from V(V) to terminal (V=O) oxygen. The UV–vis band at the same position (362 nm) is very intense for rutile $Sb_{0.95}V_{0.95}O_4$ (Fig. 2a). In the spectra of the other two samples based on SiO_2 and $NbSiO_x$ supports (Fig. 2b and d) this shoulder is not well pronounced. Instead, a broad band at about 600 nm is slightly visible. Both samples were calcined at 923 K and the broad band mentioned can be due to d–d transfer expected for V(IV) ($3d^1$) ions [23]. It suggests that the higher calcination temperature leads to a partial reduction of vanadium species, especially visible when lower content of vanadium is used (0.5VSb/$NbSiO_x$). Moreover, it should be emphasised that the samples calcined at 923 K and based on $NbSiO_x$ have the profiles of UV–vis spectra (Fig. 2d and e) suggesting also the presence of a band at ca. 330 nm typical of octahedrally coordinated V_2O_5 phase.

The presence of reduced vanadium species in the samples calcined at 923 K is confirmed by the ESR study. Fig. 3 exhibits the ESR spectra of 0.5VSb/$NbSiO_x$ and 1VSb/$NbSiO_x$ samples, revealing significant differences. Generally, various vanadium(IV) species can be detected by the ESR technique. V(IV) clusters lead to a broad signal owing to significant dipolar interactions found, e.g. in VMCM-41 samples with a high vanadium content, to which vanadium was introduced in one pot synthesis [23,26]. The isolated V(IV) species, mainly in the form of oxovanadium VO^{2+} ions, exhibit a hyperfine structure (ESR signal splits eightfold) derived from the interaction of free electrons ($3d^1$) with the magnetic nuclear moment of ^{51}V ($I = 7/2$). ESR spectra of 0.5VSb/$NbSiO_x$ (for the fresh sample $g_{II} = 1.937$ and $A_{II} = 201.4$ G), even after evacuation at 673 K (Fig. 3A), show well-resolved signals in the hyperfine structure with g and

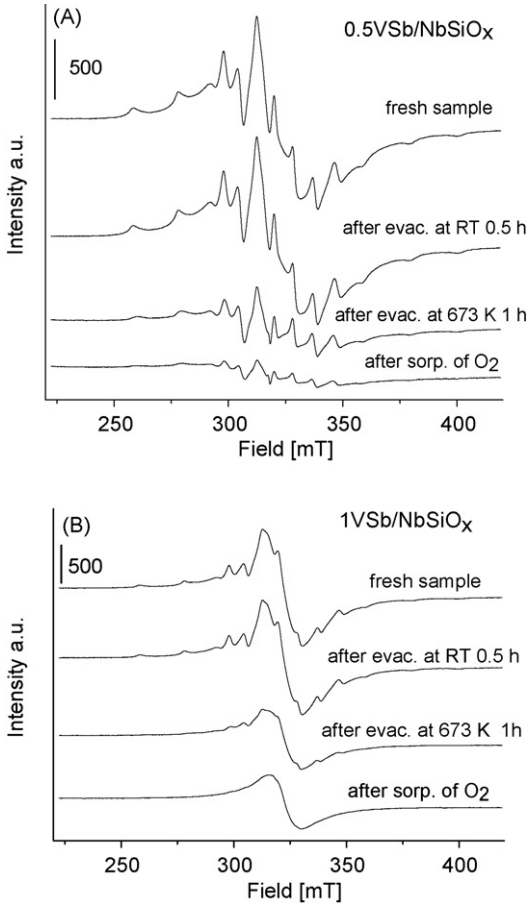

Fig. 3. ESR spectra of: (A) 0.5VSb/$NbSiO_x$ and (B) 1VSb/$NbSiO_x$ catalysts measured at 77 K.

A values characteristic of isolated VO^{2+} species. Such a structure is overlapped by a broad signal characteristic of V(IV) clusters with high vanadium content observed for 1VSb/$NbSiO_x$ (Fig. 3B), where for the fresh sample $g_{II} = 1.938$ and $A_{II} = 200.2$ G. Moreover, it is important to note that bulk compound with the rutile structure ($Sb_{0.92}{}^{5+}V_{0.8}{}^{4+}V_{0.1}{}^{3+}\square_{0.2}O_4$) and near stoichiometric $Sb^{5+}V^{4+}O_{4.5}$ exhibits also the presence of isolated VO^{2+} ions besides dimeric species [27,28]. After admission of oxygen the intensity of ESR signal from isolated VO^{2+} ions diminishes for both samples indicating the interaction between these species and gaseous oxygen. This interaction is weak and heating up to 523 K did not lead to the formation of any paramagnetic electrophilic oxygen. Short evacuation at room temperature rebuilds the pristine VO^{2+} ions. The material calcined at lower temperature (813 K) shows much lower content of VO^{2+} species which totally diminishes after evacuation at 673 K (ESR spectra not shown here).

3.2. Surface properties – FT-IR study and test reaction

Even small changes in binary oxide species on the surface of the support can affect the catalytic activity. As concerns the acidity, Lewis acid centres (LAS) and BrØnsted acid centres (BAS) were detected in the FT-IR spectra after pyridine adsorption at 373 K and desorption at various temperatures. The interaction of pyridine with Lewis acid sites leads to the appearance of bands at ~1450 and ~1610 cm^{-1} [29–31]. The intensity of the first one is related to the number of LAS whereas the position of the second band characterises the strength of LAS. Adsorption of pyridine on BrØnsted acid sites gives a band at ~1550 cm^{-1} and two other ones

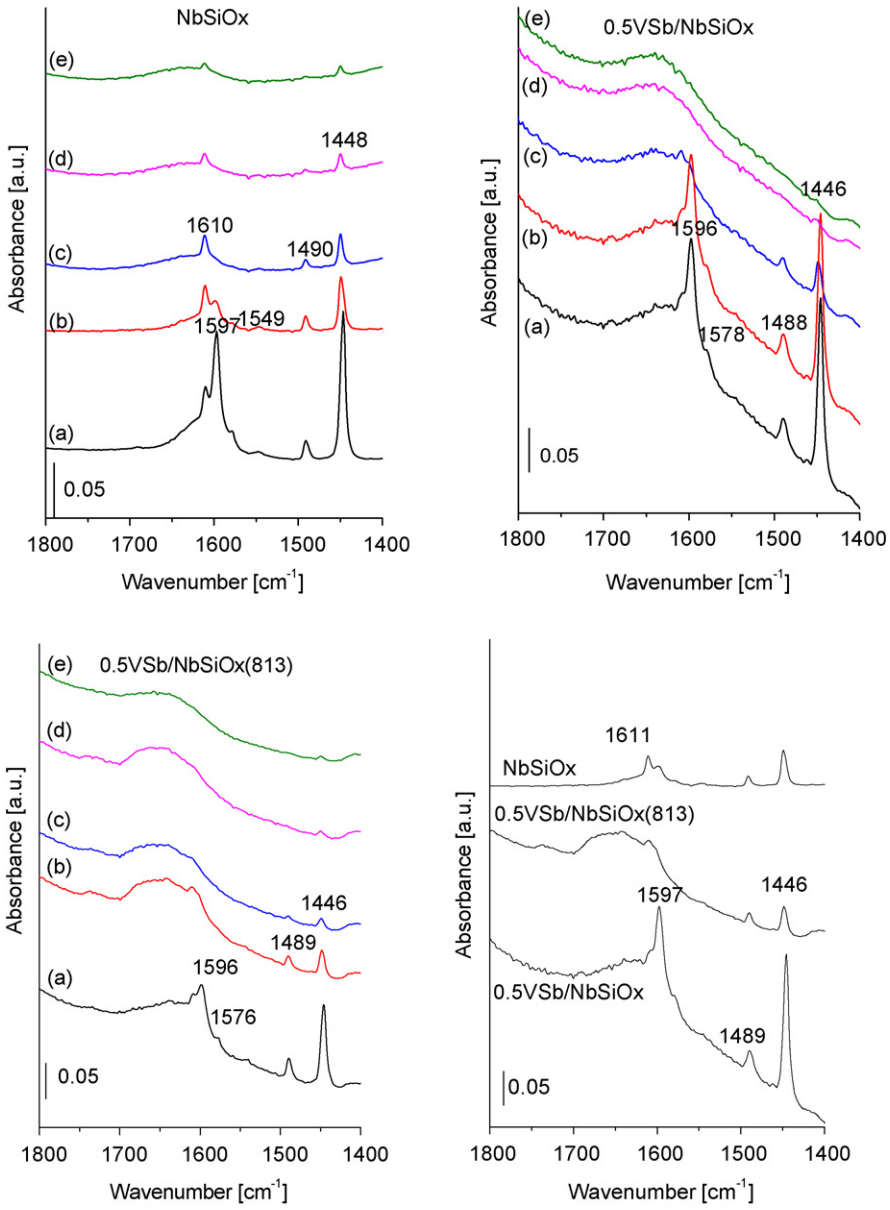

Fig. 4. Infrared spectra: (a) after pyridine adsorption at 373 K and evacuation 5 min at 373 K; (b) evacuation 0.5 h at 373 K; (c) evacuation 0.5 h at 423 K; (d) evacuation 0.5 h at 473 K; (e) evacuation 0.5 h at 523 K and comparison of the spectra after evacuation at 423 K.

in the 1620–1640 cm^{-1} range. Moreover, the bands at 1445 and 1596 cm^{-1} originate from pyridine hydrogen bonded to surface hydroxyls [31]. Fig. 4 shows that the niobiosilica $NbSiO_x$ support, after adsorption of pyridine and it evacuation at 373 K, shows acidic character. It is well visible that the band at ca. 1445 cm^{-1} overlaps the bands assigned to pyridine chemisorbed on Lewis acid sites (additional band at ca. 1610 cm^{-1}) and pyridine hydrogen bonded to hydroxyls (additional band at 1596 cm^{-1}). The evacuation at increasing temperatures causes first desorption of hydrogen bonded pyridine and next that chemisorbed on LAS. The latter is still present on the support after desorption at 473 and 523 K. It indicates that LAS exhibit high strength. Despite the presence of LAS one can observe also BrØnsted acid centres which chemisorb pyridine in the form of pyridinum cations (a broad band at ~1550 cm^{-1}). The number of Lewis acid sites decreases after modification of $NbSiO_x$ support with vanadium and antimony species as evidenced by the reduction of intensity of IR bands assigned to pyridine adsorbed on LAS (Fig. 4, band at ~1610 cm^{-1}). Interestingly, the IR bands assigned to hydrogen bonded pyridine become very intense for 0.5VSb/$NbSiO_x$ calcined at 923 K indicating the generation of new hydroxyl groups on the catalyst surface after antimony–vanadium loading on $NbSiO_x$. It is not the case for the sample containing the same vanadium and antimony amounts but calcined at the lower temperature (813 K) or the sample containing more vanadium and calcined at the same temperature (923 K). Thus it can be concluded that the vanadium–antimony loading on $NbSiO_x$ and the calcination temperature significantly modify the surface properties.

The modification mentioned can be observed in the test reactions. The cyclisation of acetonylacetone (AcOAc) was used as a test for hydroxyl basicity/acidity properties. This reaction was proposed by Dessau [32] as a test of acid–base properties. The formation of 2,5-dimethylfuran (DMF) occurs at the acidic centres, whereas the production of 3-methyl-2-cyclopentenone (MCP) takes place at the basic centres. On the basis of the selectivity MCP/DMF ratio, the sequence of basicity of catalysts studied can be proposed. According to the literature [32,33] the basicity of the catalyst is demonstrated if MCP/DMF > 1. When MCP/DMF < 1 the catalyst exhibits acidic properties, while for MCP/DMF ~ 1 the balanced acid–base prop-

Table 2
The results of acetonylacetone (AcOAc) cyclisation at 623 K.

Catalyst	AcOAc conv. [%]	Selectivity [%]		MCP/DMF
		DMF	MCP	
$NbSiO_x$	32	100	0	0
$0.5VSb/NbSiO_x$	10	81	19	0.248
$0.5VSb/NbSiO_x(813)$	7	84	16	0.198
$1VSb/NbSiO_x$	3	87	13	0.199
$0.5VSb/SiO_2$	4	84	16	0.208
$Sb_{0.95}V_{0.95}O_4$	40	18	82	4.691

MCP, 3-methyl-2-cyclopentenone; DMF, 2,5-dimethylfuran.

erties are postulated. Table 2 presents the results obtained from this test reaction. As follows, $NbSiO_x$ exhibits high activity in this reaction and the only one product – DMF is formed on BAS. It is in line with the results of pyridine adsorption presented in Fig. 4. The conversion of acetonylacetone decreases over the catalysts prepared by modification of $NbSiO_x$ with antimony and vanadium sources. Moreover, MCP is generated over $VSb/NbSiO_x$, the highest amount over $0.5VSb/NbSiO_x$ characterised by the highest concentration of surface hydroxyls estimated from pyridine adsorption and FT-IR measurements. Interestingly, bulk $Sb_{0.95}V_{0.95}O_4$ reveals the highest AcOAc conversion and the highest selectivity to MCP. The difference in the conversion and selectivity of bulk binary oxide and vanadium–antimony phase loaded on the support confirms the chemical interaction between binary vanadium–antimony oxide and the support.

3.3. Oxidation of methanol

Oxidation of methanol is a complex reaction not only interesting from the commercial point of view (production of formaldehyde) but also as a process which allows characterisation of active centres on the catalyst surface. Table 3 shows the results of oxidation of methanol performed at 473 and 523 K over all catalysts studied in this work. These results provide information on Lewis acidity and basicity as well as redox centres. The $NbSiO_x$ support gives the conversion of methanol below 10% at both temperatures and selectivity to dimethyl ether and CO_2 at 473 K. The selectivity to ether confirms the presence of acid centres detected by pyridine adsorption, whereas CO_2 formation indicates that this support contains also basic centres which at this temperature are not selective in oxidation of methanol and causes the total oxidation to CO_2. The modification of $NbSiO_x$ with vanadium–antimony binary oxides increases the methanol conversion and significantly changes the selectivity of this reaction. The considerable growth of formaldehyde formation is characteristic for all $VSb/NbSiO_x$ samples and seems to be independent of the particle sizes of rutile $Sb_{0.95}V_{0.95}O_4$ loaded phase. Fig. 5 shows the methanol conversion and selectivity to formaldehyde over the catalysts containing the same vanadium loading (0.5VSb/support) and rutile structure of various crystalline sizes. With the growth of crystalline sizes the conversion increases but the selectivity to formaldehyde is not linearly related to the size of $Sb_{0.95}V_{0.95}O_4$ crystallites. It is worth of notice that an increase in vanadium content ($1VSb/NbSiO_x$) results in a significant decrease in formaldehyde production and an increase in methylal formation at 473 K. The latter product is formed when formate species chemisorbed on LAS interact with surface oxygen and another molecule of methanol from the gas phase [3]. One should stress at this point that $1VSb/NbSiO_x$ exhibits the presence of V=O species on the surface well visible in UV–vis spectra and this species located near LAS, mainly from the support, makes the pathway for methylal formation possible [34,35]. Although, Wachs and Kim's study [36] clearly evidenced that the methanol oxidative dehydrogenation kinetic parameters were found to be independent of surface vanadium density, V=O bond length/strength, surface vanadia reduction and surface acidity, in the case of binary oxide system like $SbVO_x$ loaded on support containing niobium the mechanism seems to be more complex. Interestingly, the increase in the reaction temperature to 523 K results in a significantly higher conversion of methanol and a considerable increase in the selectivity to formaldehyde (from 43 to 81). It is because in methanol oxidation, which follows a consecutive pathway, there is a competition between the desorption of the primary product (formaldehyde) and its interaction with the neighbourhood basic surface oxygen and finally with another methanol molecule. For $1VSb/NbSiO_x$ an increase in temperature to 523 K makes the desorption of chemisorbed formaldehyde much easier than its further transformation.

Finally, the activity (Table 3) of bulk $Sb_{0.95}V_{0.95}O_4$ should be discussed. The conversion of methanol is similar to that over $1VSb/NbSiO_x$ but the selectivity to various products is totally different. The main products of the reaction over bulk $Sb_{0.95}V_{0.95}O_4$ are formaldehyde and dimethyl ether showing that both, acid Lewis and redox centres act in the form of isolated species rather than in the form of neighbouring pairs of centres.

The presented results clearly evidence that the loading of $Sb_{0.95}V_{0.95}O_4$ phase on $NbSiO_x$ significantly enhances the yield of formaldehyde. Niobium present in the support interacts with

Table 3
The results of oxidation of methanol.

Catalyst	Temperature [K]	MeOH conv. [%]	Selectivity [%]				
			HCHO	CH_3OCH_3	$HCOOCH_3$	$(CH_3O)_2CH_2$	CO_2
$NbSiO_x$	473	7	–	45	–	–	55
	523	9	25	3	69	1	2
$0.5VSb/NbSiO_x$	473	10	70	8	–	22	Traces
	523	13	81	2	12	4	1
$0.5VSb/NbSiO_x(813)$	473	10	84	3	–	10	3
	523	16	88	5	–	3	4
$1VSb/NbSiO_x$	473	11	43	5	4	46	2
	523	32	81	7	9	2	1
$0.5VSb/SiO_2$	473	4	65	5	–	27	3
	523	6	90	2	5	2	1
$Sb_{0.95}V_{0.95}O_4$	473	8	40	46	3	11	Traces
	523	34	50	43	4	3	–

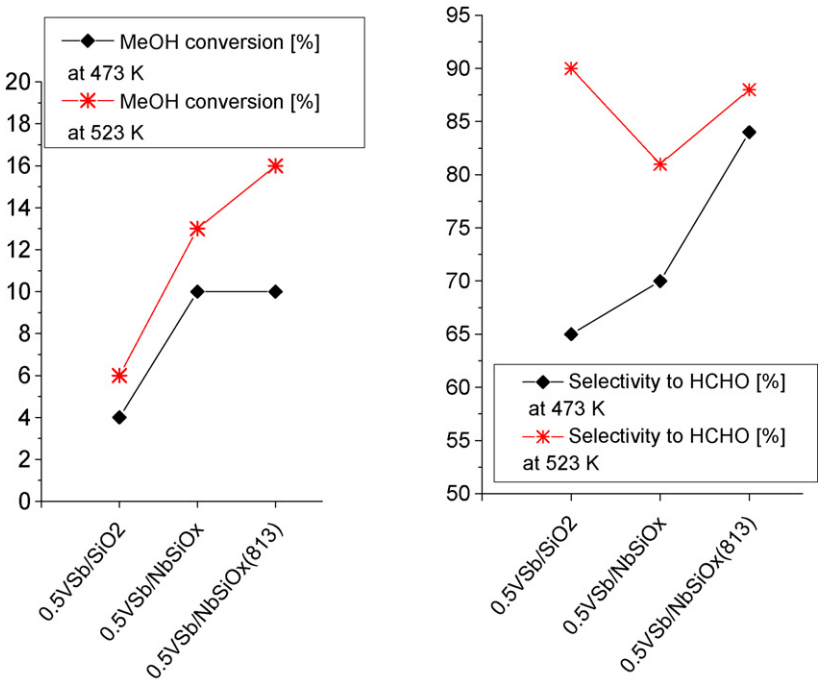

Fig. 5. Methanol conversion and selectivity to formaldehyde on the catalysts with the same V–Sb loading.

vanadium–antimony binary oxide and makes the pathway for formaldehyde production more effective.

4. Conclusions

The step by step impregnation of silica and niobiosilica supports with vanadium and antimony sources leads to generation of rutile $Sb_{0.95}V_{0.95}O_4$ phase. Vanadium–antimony binary oxide phase interacts with $NbSiO_x$ acidic surface hydroxyls and generates new OH groups exhibiting basic properties, as deduced from pyridine adsorption and acetonylacetone cyclisation. The increase in the interaction of $SbVO_x$ phase with niobium species in $NbSiO_x$ support with increasing calcination temperature results in the particle sizes of rutile phase getting smaller. The calcination temperature of $VSb/NbSiO_x$ catalysts and the content of vanadium determine also the coordination of vanadium in the samples and its oxidation state. The higher calcination temperature results in the presence of higher amount of vanadium at the +4 oxidation state, whereas the lower calcination temperature and the higher vanadium content lead to V=O species well evidenced by UV–vis spectra on the surface. The catalytic activity is determined by the surface species formed. The $Sb_{0.95}V_{0.95}O_4$ phase loading on $NbSiO_x$ support results in generation of oxidative dehydrogenation activity leading to the formation of formaldehyde in the oxidation of methanol. The presence of LAS in the neighbourhood of V=O species, for higher content of vanadium, leads to the further transformation of formaldehyde to methylal. Therefore, for the effective oxidation of methanol to formaldehyde the vanadium content in $Sb_{0.95}V_{0.95}O_4$ phase should be lower.

Acknowledgements

COST action D36, WG No D36/0006/06 and the Polish Ministry of Science (Grants Nos. 118/COS/2007/03 and N N 204 016439) are acknowledged for the financial support.

References

[1] J.M. Tatibouet, Appl. Catal. A: Gen. 148 (1997) 213.
[2] I. Sobczak, N. Kieronczyk, M. Trejda, M. Ziolek, Catal. Today 139 (2008)188.
[3] G. Busca, A.S. Elmi, P. Forzatti, J. Phys. Chem. 91 (1987) 5263.
[4] G. Busca, J. Lamotte, J.C. Lavalley, V. Lorenzelli, J. Am. Chem. Soc. 109 (1987) 5197.
[5] L.J. Burcham, I.E. Wachs, Catal. Today 49 (1999) 467.
[6] X. Gao, I.E. Wachs, M.S. Wong, J.Y. Ying, J. Catal. 203 (2001) 18.
[7] M. Muhler, in: G. Ertl, H. Knozinger, J. Weitkamp (Eds.), Handbook of Heterogeneous Catalysis, VCH, 1997, p. 2274.
[8] J. Haber, in: G. Ertl, H. Knozinger, J. Weitkamp (Eds.), Handbook of Heterogeneous Catalysis, VCH, 1997, p. 2253.
[9] L.T. Weng, P. Ruiz, B. Delmon, Stud. Surf. Sci. Catal. 72 (1992) 339.
[10] M.O. Guerrero-Pérez, M.A. Vicente, J.L.G. Fierro, M.A. Bañares, Chem. Matter 19 (2007) 6621.
[11] M.O. Guerrero-Pérez, M.A. Bañares, Appl. Catal. A 298 (2006) 1.
[12] M.O. Guerrero-Pérez, M.A. Bañares, Appl. Catal. A 139 (2008) 202.
[13] R. Grasselli, Catal. Today 99 (2005) 25.
[14] M.O. Guerrero-Pérez, J.L.G. Fierro, M.A. Vicente, M.A. Banares, J. Catal. 206 (2002) 339.
[15] H. Zhang, Z. Liu, Z. Feng, C. Li, J. Catal. 260 (2008) 295.
[16] M. Trejda, A. Tuel, J. Kujawa, B. Kilos, M. Ziolek, Microporous Mesoporous Mater. 110 (2008) 271.
[17] I. Sobczak, Catal. Today 142 (2009) 258.
[18] M. Ziolek, P. Decyk, I. Sobczak, M. Trejda, J. Florek, H. Golinska, W. Klimas, A. Wojtaszek, Appl. Catal. A, doi:10.1016/j.apcata.2010.07.022.
[19] H. Golinska, M. Ziolek, P. Decyk, J. Kujawa, E. Filipek, Catal. Today 142 (2009) 175.
[20] H. Golinska, E. Rojas, R. López-Medina, V. Calvino-Casilda, M. Ziolek, M.A. Bañares, M.O. Guerrero-Pérez, Appl. Catal. A 380 (2010) 95.
[21] P. Carniti, A. Gervasini, M. Marzo, J. Phys. Chem. C 112 (2008) 14064.
[22] I. Nowak, M. Ziolek, Stud. Surf. Sci. Catal. 165 (2007) 73.
[23] Z. Luan, J. Xu, H. He, J. Klinowski, L. Kevan, J. Phys. Chem. 100 (1996) 19595.
[24] K.J. Chao, C.N. Wu, H. Chang, L.J. Lee, Shu-fen Hu, J. Phys. Chem. B 101 (1997) 6341.
[25] M. Chatterjee, T. Iwasaki, H. Hayashi, Y. Onodera, T. Ebina, T. Nagase, Chem. Mater. 11 (1999) 1368.
[26] M. Ziolek, I. Nowak, B. Kilos, I. Sobczak, P. Decyk, M. Trejda, J.C. Volta, J. Phys. Chem. Solids 65 (2004) 571.
[27] J. Typek, E. Filipek, M. Maryniak, N. Guskos, Mater. Sci. Poland 23 (2005) 1047.
[28] J. Typek, N. Guskos, D. Buchowski, M. Wabia, E. Filipek, Radiat. Eff. Defects Solids 157 (2002) 1093.
[29] S. Khabtou, T. Chevreau, J.C. Lavalley, Microporous Mater. 3 (1994) 133.
[30] E.P. Parry, J. Catal. 2 (1963) 371.
[31] B. Chakraborty, B. Viswanathan, Catal. Today 49 (1999) 253.
[32] R.M. Dessau, Zeolites 10 (1990) 205.
[33] J.J. Alcaraz, B.J. Arena, R.D. Gillespie, J.S. Holmgren, Catal. Today 43 (1998) 89.
[34] Bell, Khaliullin, J. Phys. Chem. B 106 (2002) 7832.
[35] Sauer, Pritzche, Dobler, J. Am. Chem. Soc. 127 (2005).
[36] T. Kim, I.E. Wachs, J. Catal. 255 (2008) 197.